Application of Chemostratigraphy and Multivariate Statistical Analysis to Differentiating Bounding Stratigraphic Surfaces*

R.A. Eisenberg[1] and R.M. Harris[2]

Search and Discovery Article #60042 (2009)
Posted June 1, 2009

*Reprint from Eisenberg, R.A., and P.M. Harris, 1995, Application of chemostratigraphy and multivariate statistical analysis to differentiating bounding stratigraphic surfaces, *in* P.H. Pausé and M.P. Candelaria, eds., Carbonate Facies and Sequence Stratigraphy: Practical Applications of Carbonate Models: Permian Basin Section-SEPM Publication 95-36 / Permian Basin Graduate Center Publication 5-95, p. 83-102. Appreciation is expressed to PBS-SEPM (http://www.pbssepm.org/mainframe.htm) and to Paula Mitchell, Executive Director, for permission to post this article.

[1]Chevron Petroleum Technology Company, LaHabra, CA; currently Chevron International Exploration and Production Company (raei@chevron.com)
[2]Chevron Petroleum Technology Company, LaHabra, CA; currently ETC, Chevron, San Ramon, CA, USA. (MitchHarris@chevron.com)

Abstract and Contents

Abstract

Outcrops of the Permian San Andres Formation along the western edge of the Guadalupe Mountains of southeastern New Mexico have been thoroughly studied from a stratigraphic perspective, but some uncertainty remains in specifically identifying certain bounding surfaces (sequence boundaries, cycle boundaries,and flooding surfaces). We have tested the application of multielement geochemistry on core samples to further define the bounding surfaces within this cyclic ramp carbonate framework.

Five stratigraphic intervals were sampled from two cored wells drilled adjacent to the outcrops. Major, minor, trace, and rare earth elements were measured by a commercial laboratory on 44 composites taken across 5 stratigraphic bounding surfaces. Significant variations of individual elements are observed across some of the bounding surfaces. Interrelationships between 25 chemical variables were examined using multivariate statistics. Principal components analysis, performed on centered log ratios of the compositional variables, yielded five principal components with eigenvalues greater than one and which explained eighty-one percent of the variance of the data. Clustering of variables was investigated through varimax rotation of the principal components (factor analysis). Utilizing this technique, three factors related to depositional/diagenetic processes were interpreted and used to evaluate the five bounding stratigraphic surfaces.

Relatively high concentrations of elements associated with a “detrital clay factor” occur within two cycle boundaries coincident with the transition of the middle to upper San Andres and may represent a sequence boundary. Concentration of organic carbon and associated base metals coincides with a flooding surface and occurs at the transition from outer ramp to cyclic ramp crest deposition. Our approach may have utility in defining a

Copyright © AAPG. Serial rights given by author. For all other rights contact author directly.

stratigraphic framework from downhole log and cuttings data where some criteria for recognizing bounding surfaces cannot easily be used.

Contents

APPLICATION OF CHEMOSTRATIGRAPHY AND MULTIVARIATE STATISTICAL ANALYSIS TO DIFFERENTIATING BOUNDING STRATIGRAPHIC SURFACES

RICHARD A. EISENBERG and PAUL M. HARRIS
Chevron Petroleum Technology Company
1300 Beach Boulevard,La Habra, California 90633

ABSTRACT

Outcrops of the Permian San Andres Formation along the western edge of the Guadalupe Mountains of southeastern New Mexico have been thoroughly studied from a stratigraphic perspective, but some uncertainty remains in specifically identifying certain bounding surfaces (sequence boundaries, cycle boundaries, and flooding surfaces). We have tested the application of multielement geochemistry on core samples to further define the bounding surfaces within this cyclic ramp carbonate framework.

Five stratigraphic intervals were sampled from two cored wells drilled adjacent to the outcrops. Major, minor, trace and rare earth elements were measured by a commercial laboratory on 44 composites taken across 5 stratigraphic bounding surfaces. Significant variations of individual elements are observed across some of the bounding surfaces. Interrelationships between 25 chemical variables were examined using multivariate statistics. Principal components analysis, performed on centered log ratios of the compositional variables, yielded five principal components with eigenvalues greater than one and which explained eighty one percent of the variance of the data. Clustering of variables was investigated through varimax rotation of the principal components (factor analysis). Utilizing this technique, three factors related to depositional/diagenetic processes were interpreted and used to evaluate the five bounding stratigraphic surfaces.

Relatively high concentrations of elements associated with a "detrital clay factor" occur within two cycle boundaries coincident with the transition from the middle to upper San Andres and may represent a sequence boundary. Concentration of organic carbon and associated base metals coincides with a flooding surface and occurs at the transition from outer ramp to cyclic ramp crest deposition. Our approach may have utility in defining a stratigraphic framework from downhole log and cuttings data where some criteria for recognizing bounding surfaces can not easily be used.

GEOLOGIC SETTING

Our study area is the Lawyer Canyon locality of the Algerita Escarpment in the Guadalupe Mountains. Previous studies have shown that these outcrops have stratigraphic relations similar to those found within many reservoirs in the Permian Basin (Sarg and Lehmann, 1986; Grant and others, 1994; Kerans and others, 1994; Eisenberg and others, 1994) and therefore are valuable as analogs in reservoir studies.

The outcrops along the Algerita Escarpment consist of dolomitized carbonate-ramp facies that have been described in detail by Kerans and others (1994). As a result of the shifts of facies tracts that occurred during San Andres deposition, deposits of inner ramp, ramp crest and outer ramp origin are commonly stacked vertically at any one outcrop locality. A sequence stratigraphic framework for these outcrops was developed by Sarg and Lehmann (1986) and Sarg and others (1988), then subsequently modified substantially by Kerans and others (1991, 1992, 1994). The San Andres consists of two large-scale sequences that can be further subdivided into smaller-scale sequences and their component depositional cycles (Kerans and others, 1994).

Our core descriptions (Fig. 1) show the geologic variation found in a portion of the middle and upper San Andres at the Lawyer Canyon locality. The cored wells, Algerita #1 and #3, were drilled at distances ranging from 183 to 262 m (600 to 860 ft) behind the outcrop face and 372 m (1220 ft) from each other. The depositional facies, stratigraphy, and permeability distribution were documented for these wells by Grant and others (1994) and Eisenberg and others (1994). The lower part of the section shown on Figure 1 consists of fusulinid-rich facies with depositional cycles developed to varying degrees (Units BGZ, FUZ and MFZ of Eisenberg and others, 1994). Larger scale 'cyclicity' is reflected by a progressive upward thinning then thickening of bedding. These deposits change upward into more distinctly bedded and cyclic subtidal fusulinid facies (Cycles P1-4) that are then overlain by stacked, well-developed, ooid-capped shoaling cycles (Cycles 1-9 of Kerans and others, 1994; and Grant and others, 1994).

METHODS

Multielement geochemical analysis was performed on cores from the two wells drilled adjacent to the Lawyer

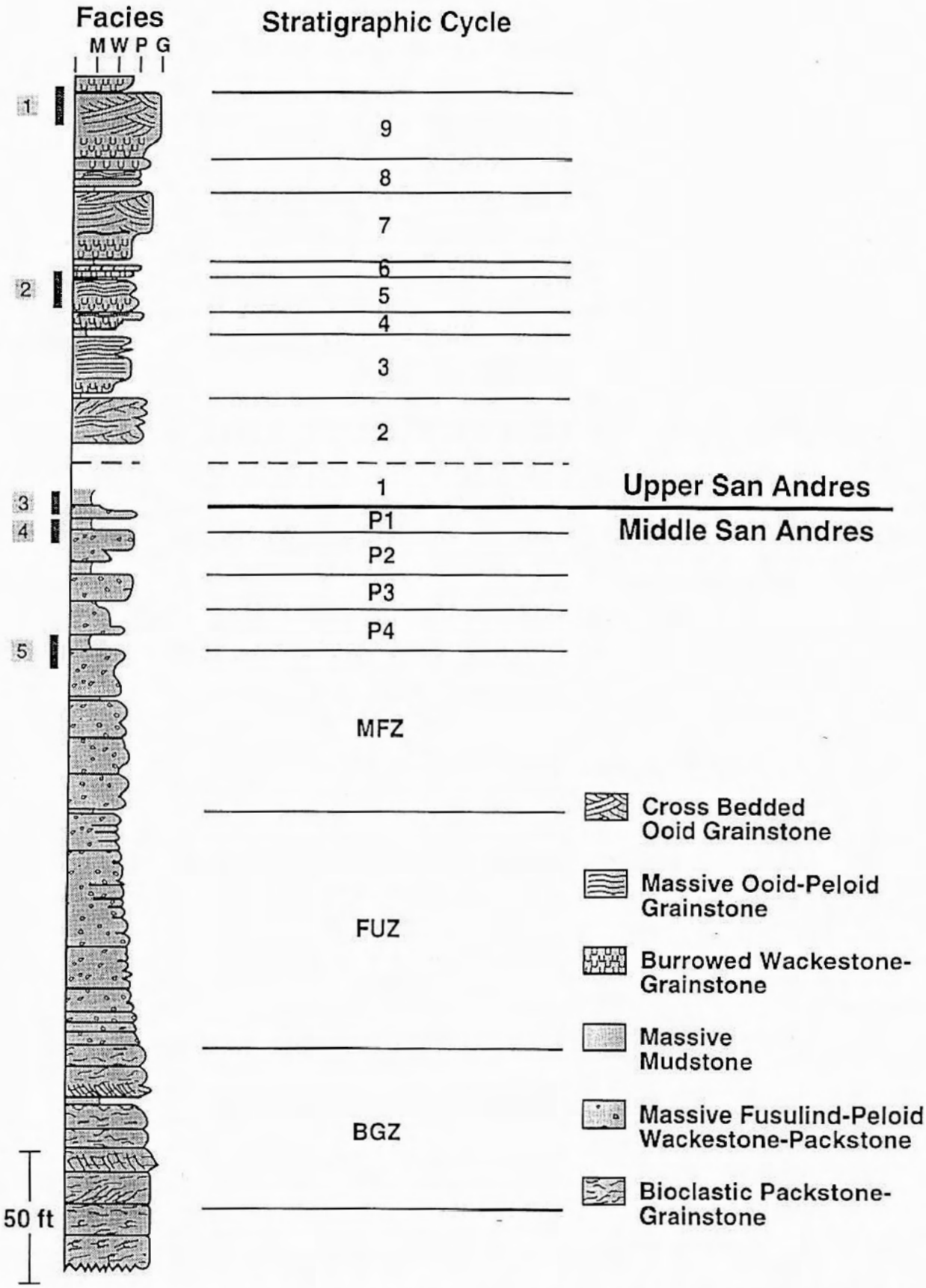

FIGURE 1. Graphic log of core descriptions for the Algerita #1 and #3 cores from Lawyer Canyon locality of Algerita Escarpment showing stratigraphic intervals 1 - 5 that were sampled for this study. Facies and cycles recognized in the cores are described in more detail by Grant and others (1994) and Eisenberg and others (1994).

TABLE 1. Decription of stratigraphic intervals sampled in the Algerita #1 and #3 cores for chemostratigraphy analysis.

SAMPLES FOR MULTIELEMENT GEOCHEMICAL ANALYSIS WERE COLLECTED ACROSS FIVE STRATIGRAPHIC BOUNDING SURFACES

Interval 1. Cycle and Small-Scale Sequence Boundary
Surface 1 is a boundary between two depositional cycles (Cycles 9 and 10). Cycle 9 contains a facies succession indicating upward shoaling deposition (Kerans and others, 1994; Harris and others, 1994; Hovorka and others, 1994). The cycle boundary is also coincident with a sequence boundary (between small-scale sequences G3 and 4 of Kerans and others, 1994) based on major offset of the facies tracts and localized evidence of paleokarst.

Interval 2. Cycle Boundary and Flooding Surface
Surface 2 is a boundary between two depositional cycles that are relatively thin. The cycle boundary may also be a flooding surface based on cycle stacking pattern and facies composition, as proposed by Kerans and others (1994) within their small-scale sequence G3.

Interval 3. Cycle and Possible Sequence (Large- and Small-Scale) Boundary
Surface 3 is a boundary between two depositional cycles (Cycle P1 and 1). Both cycles are relatively thick with muddier bases and more grain-rich tops; the upper cycle is more demonstrably an upward shoaling succession of facies. The cycle boundary coincides with the large-scale sequence boundary defined by Sarg and Lehmann (1986) and also recognized by Sarg and others (1988) and Kerans and others (1991). Cycle P1 shows no evidence of local subaerial exposure and there is no paleokarst recognized with the sequence boundary. Evidence for the sequence boundary as proposed by Sarg and Lehmann (1986) was facies offset and the interpretation that the boundary was a bypass surface for siliciclastics to the basin that lie further south. Kerans and others (1992, 1994) moved this particular boundary upward since little evidence supported its position here: a) no upward shoaling or paleokarst; b) only minor facies offset; c) no stacking pattern or facies composition criteria; and d) more refined shelf-to-basin correlation indicating that this surface is not a bypass surface. With this interpretation, our Surface 3 occurs within the highstand systems tract of both a small-scale and large-scale sequence as defined by Kerans and others (1994)(small-scale sequence G2 and their large-scale lower San Andres depositional sequence).

Interval 4. Cycle Boundary
Surface 4 is a boundary between two depositional cycles (P1 and 2). The cycles are relatively thick, fusulinid-rich subtidal cycles with little evidence for upward shoaling and no evidence of subaerial exposure. The boundary occurs within the highstand systems tract of a small-scale (sequence G2) and large-scale sequence (lower San Andres depositional sequence) as defined by Kerans and others (1994).

Interval 5. Cycle Boundary and Possible Flooding Surface
Surface 5 is a boundary between a well-developed subtidal depositional cycle (P4) and the underlying depositional unit (MFZ) of Goggin and others (1993) and Eisenberg and others (1994) consisting of thick-bedded but poorly developed cycles. The boundary occurs within the lower portion of the highstand systems tract of small-scale sequence G2 defined by Kerans and others (1994).

Canyon outcrops. Samples across five bounding stratigraphic surfaces were selected (Table 1). Interval composite samples, broken out by lithology, were selected to give near continuous sample coverage across the five stratigraphic surfaces. All five intervals examined in this study contain boundaries of small-scale depositional cycles, but not all of the cycles occur within the same portions of larger-scale sequences. Some of the cycle boundaries are (or may be) coincident with sequence boundaries (intervals 1 and 3), whereas others coincide with flooding surfaces (intervals 2 and 5).

A total of 44 samples from the five intervals were analyzed for major, minor, trace and REE using a combination of techniques including inductively coupled plasma (ICP) and mass spectrometry (Table 2). Data below detection limits was discarded before tabulation and statistical analysis. Multivariate statistical analysis of the chemical data was conducted on a Macintosh IIci computer

TABLE 2. Multielement geochemical data generated for the Algerita #1 and #3 cores. A total of 44 samples from the five stratigraphic intervals were analyzed for major, minor, trace and REE using a combination of techniques including inductively coupled plasma (ICP) and mass spectrometry.

WELL#	Ft_From	Ft_To	Interval	Para	Para_Dist	SiO2%	Al2O3%	Fe2O3%	MgO%	CaO%	Na2O%	K2O%	TiO2%	P2O5%	Cr2O3%	C_TOT%
ALG#1	182.9	184	1	USA10	0.55	0.68	0.08	0.1	20.79	31.08	0.07	0.16	0.01	0.07	0.002	13.32
ALG#1	184	184.2	1	USA9	-0.1	0.52	0.1	0.09	21.55	30.71	0.05	0.13	0.01	0.07	0.002	12.31
ALG#1	185	186	1	USA9	-1.5	0.19	0.03	0.02	21.1	29.63	0.11	0.09	0.01	0.07	0.002	12.57
ALG#1	187	187.7	1	USA9	-3.35	0.2	0.03	0.02	20.9	29.49	0.13	0.16	0.01	0.09	0.002	12.54
ALG#1	188.8	190.3	1	USA9	-5.55	0.16	0.01	0.04	21.21	29.65	0.05	0.05	0.01	0.06	0.002	12.6
ALG#1	190.3	191	1	USA9	-6.65	0.37	0.01	0.06	21.18	30.12	0.05	0.1	0.01	0.06	0.002	12.71
ALG#1	191.7	192.2	1	USA9	-7.95	0.67	0.01	0.04	20.96	29.4	0.12	0.18	0.01	0.06	0.002	12.56
ALG#1	194	194.6	1	USA9	-10.3	0.3	0.01	0.03	20.75	29.76	0.06	0.05	0.01	0.06	0.002	12.86
ALG#1	196	197	1	USA9	-12.5	0.38	0.03	0.05	20.9	30.35	0.08	0.09	0.01	0.06	0.002	12.9
ALG#1	197	198	1	USA9	-13.5	0.23	0.01	0.03	21.18	30.1	0.11	0.15	0.01	0.06	0.002	12.82
ALG#1	252.3	252.7	2	USA6	2	0.35	0.04	0.09	21.09	31.13	0.05	0.11	0.01	0.09	0.01	12.64
ALG#1	253	253.7	2	USA6	1.15	0.25	0.01	0.05	21.29	31.21	0.05	0.08	0.01	0.05	0.002	13.09
ALG#1	254	254.5	2	USA6	0.25	0.48	0.06	0.06	21.1	31.25	0.05	0.18	0.01	0.06	0.002	12.97
ALG#1	255	255.8	2	USA5	-0.9	0.4	0.1	0.03	21.54	30.73	0.06	0.05	0.01	0.06	0.002	12.63
ALG#1	256	256.5	2	USA5	-1.75	0.26	0.05	0.03	21.14	30.64	0.12	0.24	0.01	0.06	0.003	12.95
ALG#1	257	258.7	2	USA5	-3.35	0.37	0.1	0.03	21.31	30.56	0.08	0.15	0.01	0.05	0.002	12.81
ALG#1	259	260.1	2	USA5	-5.05	0.47	0.12	0.05	21.28	30.86	0.07	0.23	0.01	0.06	0.002	12.87
ALG#1	261	261.6	2	USA5	-6.8	0.19	0.03	0.05	21.42	30.91	0.08	0.12	0.01	0.06	0.002	13.05
ALG#1	262	262.4	2	USA5	-7.7	0.36	0.07	0.06	19	33.37	0.05	0.22	0.01	0.06	0.002	12.74
ALG#1	263	263.7	2	USA5	-8.85	0.27	0.06	0.07	18.02	34.77	0.05	0.13	0.01	0.04	0.002	12.79
ALG#1	264.9	265.5	2	USA5	-10.7	0.68	0.2	0.09	19.75	32.38	0.05	0.25	0.01	0.05	0.002	12.64
ALG#1	336.3	337	3	USA1	4.35	2.84	0.67	0.31	20.06	29.93	0.05	0.35	0.06	0.11	0.002	12.31
ALG#1	338	338.6	3	USA1	2.7	1.07	0.25	0.11	21.05	30.58	0.05	0.3	0.01	0.05	0.002	12.91
ALG#1	340	340.5	3	USA1	0.75	0.97	0.22	0.06	21.41	30.36	0.06	0.21	0.01	0.04	0.002	12.87
ALG#1	341	341.4	3	MSA1	-0.2	0.39	0.04	0.05	20.31	31.53	0.09	0.23	0.01	0.03	0.003	12.9
ALG#1	342	343.1	3	MSA1	-1.55	0.46	0.03	0.08	19.05	32.91	0.07	0.19	0.01	0.05	0.007	12.7
ALG#1	343.75	345.1	3	MSA1	-3.43	0.56	0.07	0.07	18.63	33.33	0.05	0.28	0.01	0.05	0.003	13.04
ALG#1	346	347.25	4	MSA1	-5.63	0.83	0.18	0.11	20.69	30.88	0.09	0.3	0.01	0.06	0.003	12.6
ALG#1	347.25	347.6	4	MSA1	3.32	1.07	0.25	0.14	20.9	30.61	0.05	0.11	0.01	0.05	0.002	12.76
ALG#1	349	350.75	4	MSA1	0.88	1.73	0.49	0.15	20.81	30.23	0.05	0.16	0.02	0.04	0.002	12.76
ALG#1	350.8	351.2	4	MSA2	-0.25	3.49	1.73	0.65	15.61	33.15	0.1	0.98	0.08	0.07	0.007	12.15
ALG#1	351.2	351.75	4	MSA2	-0.73	1.31	0.41	0.13	20.84	30.32	0.06	0.41	0.02	0.05	0.002	12.79
ALG#1	352	354	4	MSA2	-2.25	0.27	0.01	0.03	20.79	31.15	0.07	0.21	0.01	0.04	0.002	12.75
ALG#1	355.5	356.75	4	MSA2	-5.38	0.57	0.01	0.05	18.14	33.8	0.09	0.24	0.01	0.04	0.003	12.73
ALG#3	390.9	392.25	5	MSA4	4.43	0.57	0.06	0.09	20.44	31.75	0.09	0.1	0.01	0.05	0.003	12.96
ALG#3	392.4	393.4	5	MSA4	3.1	0.4	0.04	0.06	21.36	31.28	0.06	0.13	0.01	0.03	0.002	12.75
ALG#3	393.5	394.25	5	MSA4	2.13	1.07	0.18	0.09	21.48	30.58	0.09	0.19	0.01	0.06	0.003	12.75
ALG#3	394.25	396	5	MSA4	0.88	1.28	0.4	0.17	21.19	30.55	0.05	0.06	0.02	0.06	0.002	12.76
ALG#3	397	398	5	MSA5	-1.5	0.64	0.07	0.21	20.23	31.15	0.11	0.15	0.01	0.05	0.004	12.85
ALG#3	398	399	5	MSA5	-2.5	0.42	0.01	0.11	21.39	30.16	0.11	0.27	0.01	0.05	0.003	13
ALG#3	399	399.75	5	MSA5	-3.38	0.42	0.02	0.12	21.49	30.16	0.09	0.05	0.01	0.05	0.002	13.07
ALG#3	399.75	401.2	5	MSA5	-4.48	0.77	0.07	0.1	21.48	30.11	0.05	0.05	0.01	0.06	0.002	12.97
ALG#3	402	403	5	MSA5	-6.5	0.57	0.06	0.1	21.62	30.48	0.05	0.05	0.01	0.03	0.002	12.91
ALG#3	404.2	405.5	5	MSA5	-8.85	0.39	0.04	0.04	21.67	30.23	0.09	0.05	0.01	0.06	0.002	12.88

ORG%	CO2%	LOI%	Bappm	Srppm	Lappm	Yppm	Zrppm	Nbppm	Cuppm	Pbppm	Zappm	Nippm	Asppm	Vppm
0.03	48.65	46.9	29	85	21	2	8	49	1	4	8	1	3	3
0.01	45	46.7	32	88	22	2	5	44	1	8	13	1	2	6
0.03	45.88	48.7	21	107	29	3	10	67	1	2	5	1	2	2
0.03	45.77	48.9	23	105	43	3	22	73	1	8	3	1	2	2
0.02	46.02	48.8	5	100	19	3	5	42	1	3	1	1	2	1
0.02	46.44	48	10	89	24	3	9	61	1	4	2	1	2	2
0.02	45.88	48.5	5	101	22	3	7	54	1	3	2	1	2	2
0.02	46.98	49	5	100	14	2	5	44	1	4	1	1	2	1
0.01	47.13	48	18	95	12	4	20	39	1	7	1	1	2	2
0.02	46.77	48.1	5	98	6	4	12	26	1	4	1	1	2	1
0.01	46.2	47	5	84	21	3	11	31	1	5	1	1	2	2
0.02	47.88	47	5	88	10	3	10	41	11	7	2	1	2	1
0.02	47.39	46.7	7	82	30	3	34	66	1	7	1	1	2	4
0.03	46.15	47	5	101	23	3	6	42	1	5	1	1	2	2
0.03	47.29	47.4	10	107	11	2	19	37	1	2	1	1	2	5
0.03	46.75	47.3	5	99	8	2	8	25	1	2	1	1	2	2
0.03	46.96	46.8	5	84	15	3	23	28	1	7	1	1	2	3
0.01	47.62	47.1	5	82	16	2	14	47	1	4	1	1	3	3
0.01	46.58	46.8	82	91	22	3	14	52	1	4	1	1	3	2
0.02	46.72	46.6	5	101	9	2	5	20	1	2	1	1	3	3
0.02	46.19	46.5	130	83	18	3	11	33	1	4	1	1	3	3
0.05	44.82	45.5	204	124	4	4	363	20	1	6	4	4	6	9
0.04	47.01	46.5	5	93	9	3	64	50	1	3	1	3	3	5
0.04	46.87	46.6	5	92	19	4	14	53	1	4	1	1	3	5
0.04	46.76	47.3	5	92	4	6	5	20	1	2	1	1	2	2
0.03	46.2	47.1	5	90	16	4	8	38	1	4	1	2	3	2
0.05	47.31	46.9	5	89	18	3	14	41	1	5	1	1	3	3
0.04	45.97	46.8	5	87	10	2	8	35	1	5	1	2	3	5
0.03	46.55	46.8	141	92	4	2	5	20	1	6	1	2	3	5
0.04	46.48	46.3	96	109	9	2	8	37	1	4	1	3	4	7
0.04	44.31	44	243	145	18	6	114	35	3	9	8	9	10	17
0.04	46.56	46.4	18	91	9	5	11	23	1	2	1	3	4	5
0.04	46.3	47.4	11	76	6	5	5	38	1	5	1	1	2	3
0.04	46.42	47	21	83	18	4	9	40	1	5	13	1	2	4
0.06	47.26	46.8	16	90	4	6	5	20	4	24	44	1	2	7
0.05	46.22	46.6	5	82	4	3	5	20	2	17	45	1	2	4
0.05	46.46	46.2	57	91	9	4	5	20	4	23	49	3	3	2
0.05	46.54	46.2	29	105	15	5	5	20	3	15	30	3	4	4
0.06	46.79	47.3	36	83	4	4	5	20	7	62	307	3	2	2
0.04	47.36	47.4	29	83	4	3	5	20	6	38	217	2	2	3
0.06	47.62	47.6	13	83	4	4	5	20	6	38	226	2	2	6
0.06	47.19	47.3	17	74	5	4	5	20	4	30	142	2	2	5
0.07	46.89	47	5	87	4	5	5	20	6	33	110	3	2	7
0.07	46.82	47.4	5	91	7	5	5	20	2	12	31	2	2	7

using Version 3.0.2 of JMP Statistical Visualization Software (SAS Institute Inc.) to investigate interrelationships between the various chemical variables. Principal component analysis was used to investigate the arrangement of samples across multiple correlated variables and picture the structure of the data as completely as possible using as few variables as possible. Log ratios were utilized to avoid results influenced by the constant-sum constraint imposed by the analytical data.

RESULTS

Variations of selected elements are observed when plotted against depth and lithology/texture for some of the stratigraphic intervals that straddle a bounding surface (Figs. 2a-e). For example, variations of several elements occur within intervals 3 and 4 (Fig. 2c and d). These variations do not occur, however, at the same stratigraphic position in each case relative to the boundary. Although this simplified plotting approach to characterizing surfaces has value, it is extremely difficult for one to assess the relative importance of variations of the different elements and to recognize significant covariation. Therefore, we have attempted to more fully investigate chemical covariance through multivariate statistical analysis of the data.

The results of our principal components analysis are shown as Table 3. Five principal components with eigenvalues greater than one explain 81 percent of the variance in the data. Analysis of the first three principal components was used to help discriminate between the different chemical signatures of the five intervals and identify outlying sample groups. Rotation of these three principal components identified the chemically unique nature of interval 5 .

Clustering of the chemical variables was investigated through varimax rotation of the principal components. A table of rotated principal components (Table 4) shows factor loadings of the chemical variables. Three of the principal components displayed within the table can be related to depositional and diagenetic processes. The first (Factor 1) loads on Si, Al, Fe, Ti, Ba, Ni, As, and V which we interpret to represent an introduction of detrital-clay; a second (Factor 3) loads on Ca and Mg which we relate to dolomitization; and a third (Factor 4) can be related to organo-metallic complexing and loads on Cu, Pb, Zn and organic carbon.

Figures 3a-e are plots showing the variation with depth of the rotated principal components (1 = detrital clay factor, 3 = dolomite factor, and 4 = organo-metallic factor) across each of the five stratigraphic bounding surfaces.

- Factor loadings on each of the three rotated principal components change abruptly across interval 1 which is a cycle boundary that coincides with a sequence boundary of Kerans and others (1994). Significant trends are not apparent within the underlying cycle as the boundary is approached.
- In contrast, a more systematic trend (decreasing followed by increasing) with regard to principal component 1 occurs across interval 2, a flooding surface as proposed by Kerans and others (1994). Principal components 3 and 4 show an abrupt change across this same boundary.
- Principal components 1 and 3 change abruptly across interval 3, whereas component 4 changes very little.
- All three rotated principal components change significantly across interval 4 which is a cycle boundary in the upper portion of a sequence. Intervals 3 and 4 are at and just below, respectively, a major sequence boundary as proposed by Sarg and Lehmann (1986).
- Variations of the principal components across interval 5, which is at approximately at the position of a flooding surface within a sequence proposed by Kerans and others (1994), are not uniform. The first changes abruptly, the second shows a significant change just below and at the boundary, and the third changes across and again above the boundary.

Using an approach of multielement geochemistry, multivariate statistics, and unique plotting of the data, we are able to chemically fingerprint the different stratigraphic boundaries and interpret depositional processes occurring across them. As an example of the better definition of a boundary, note that appreciable variation of elements associated with rotated component 1, the "detrital-clay factor", occur within stratigraphic intervals 3 and 4 (compare Figure 2c and d with Figure 3c and d, respectively). These intervals straddle the transition from middle to outer ramp deposition, are coincident with the transition from the middle to upper San Andres, and may represent a large-scale sequence boundary as proposed by Sarg and Lehmann (1986). Also, elevated concentrations of organic carbon and associated base metals represented by rotated component 4, the "organo-metallic factor", are found within stratigraphic interval 5 at the transition from outer ramp to cyclic ramp-crest deposition, which coincides with a flooding surface in the middle San Andres and within sequence G2 of Kerans and others (1994) (compare Figures 2e and 3e). We have not yet examined the organic composition to evaluate possible sources. We suspect the base metals are introduced during later diagenesis and are abundant due to organic complexing.

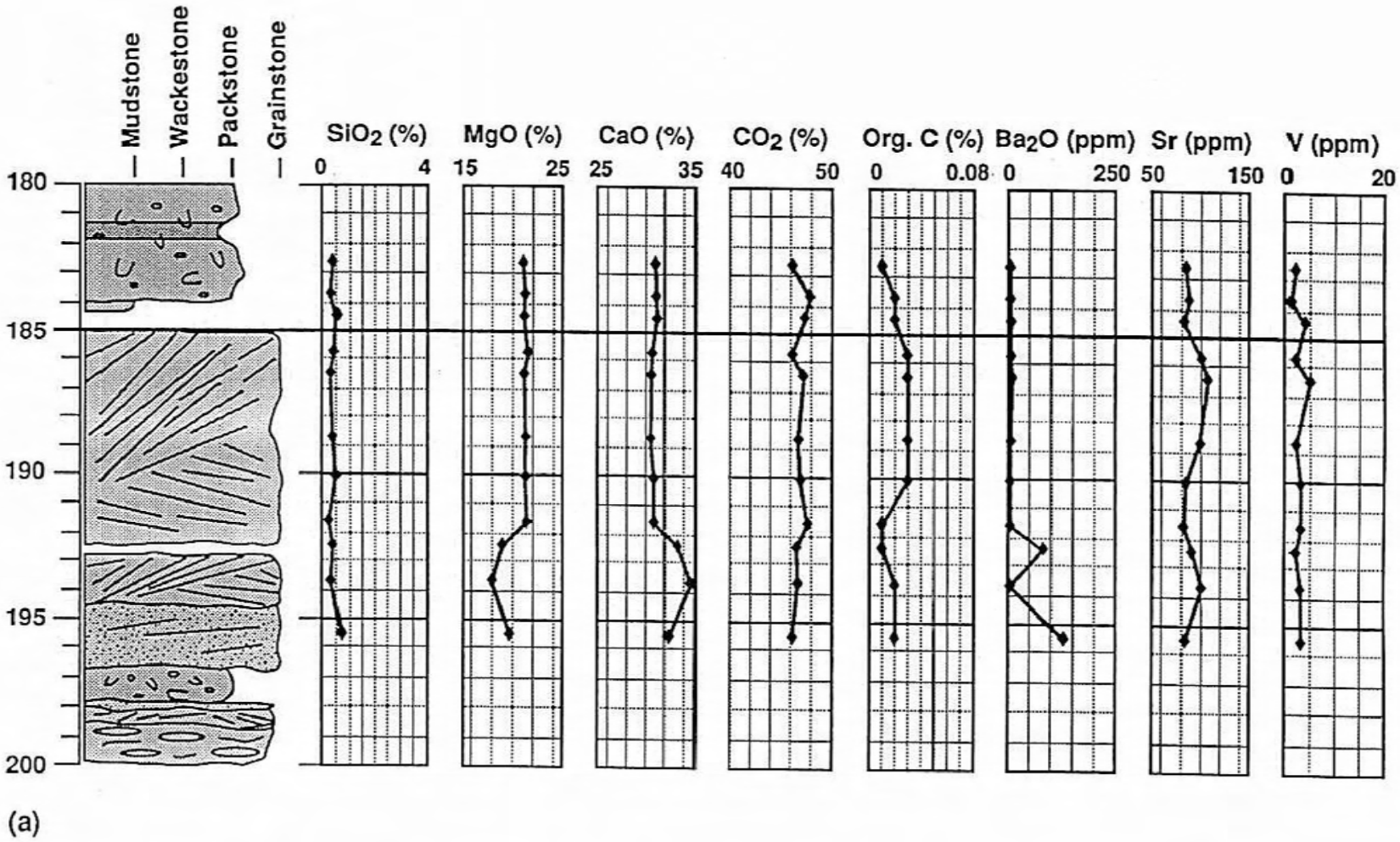

FIGURE 2a. Depth plots of key elements for each of the sampled stratigraphic intervals in the core (interval 1). Depositional textures and sedimentary structures are like those shown on Figure 1. The boundary between depositional cycles is indicated by a bold line.

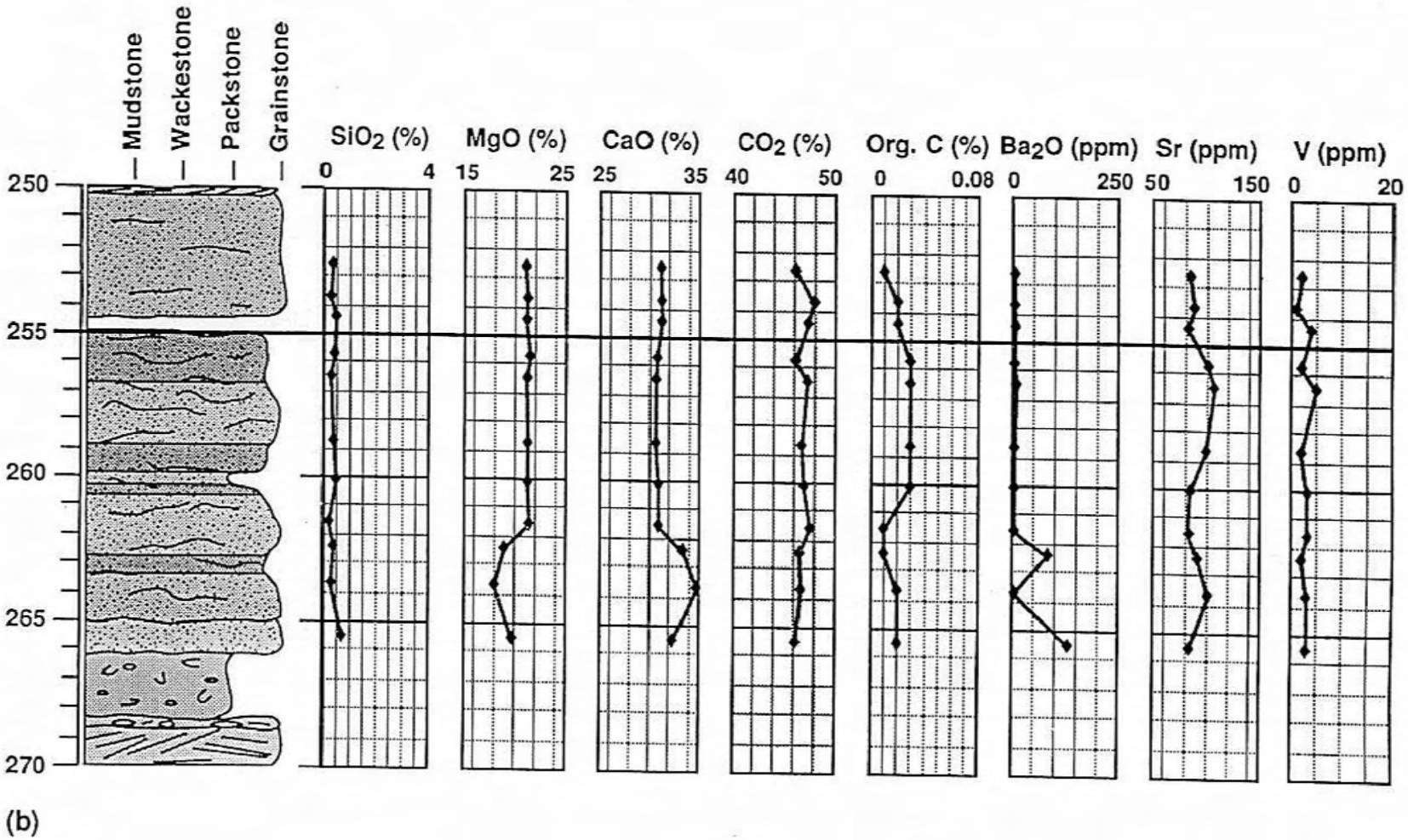

FIGURE 2b. Depth plots of key elements for each of the sampled stratigraphic intervals in the core (interval 2). Depositional textures and sedimentary structures are like those shown on Figure 1. The boundary between depositional cycles is indicated by a bold line.

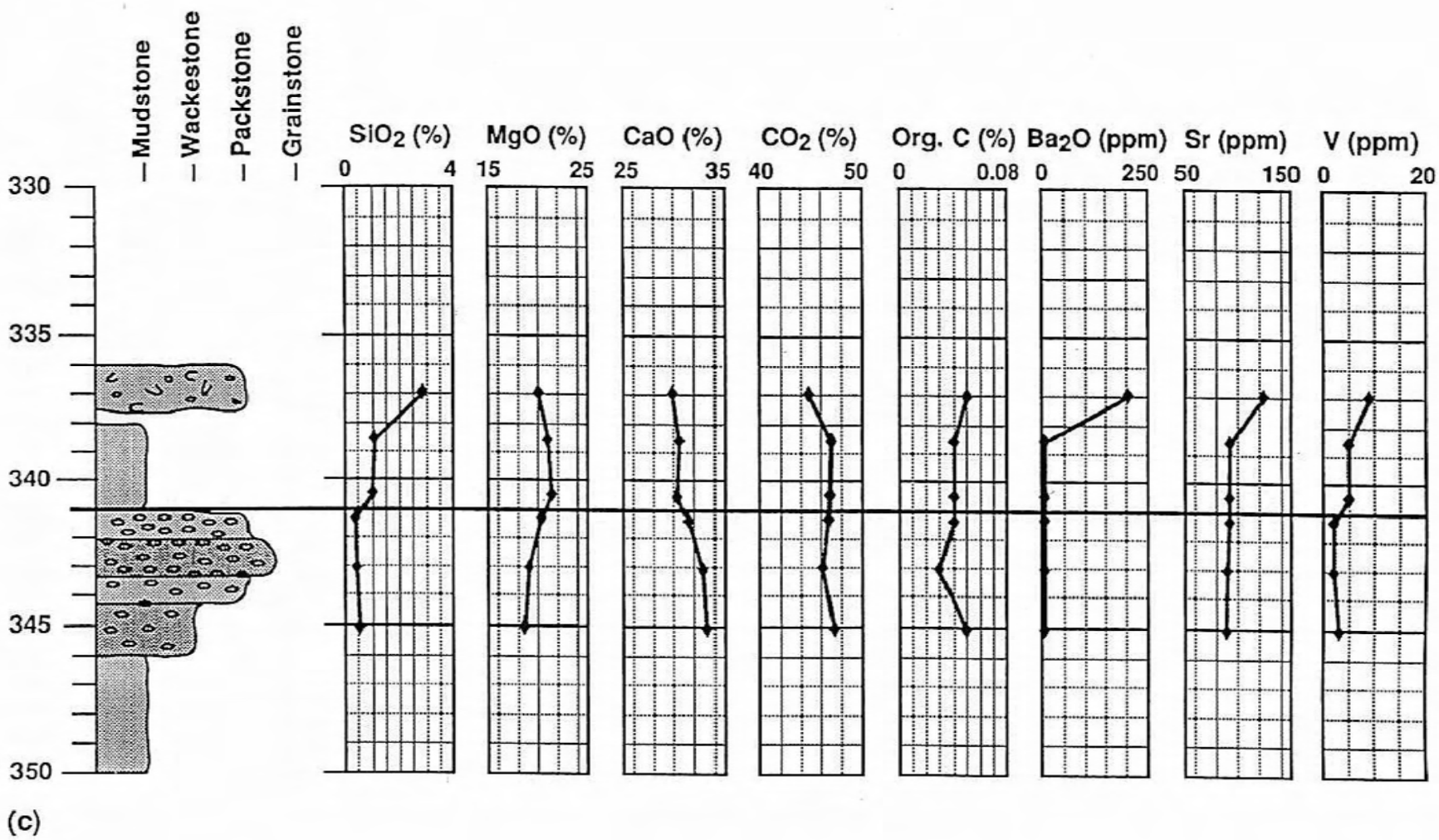

FIGURE 2c. Depth plots of key elements for each of the sampled stratigraphic intervals in the core (interval 3). Depositional textures and sedimentary structures are like those shown on Figure 1. The boundary between depositional cycles is indicated by a bold line.

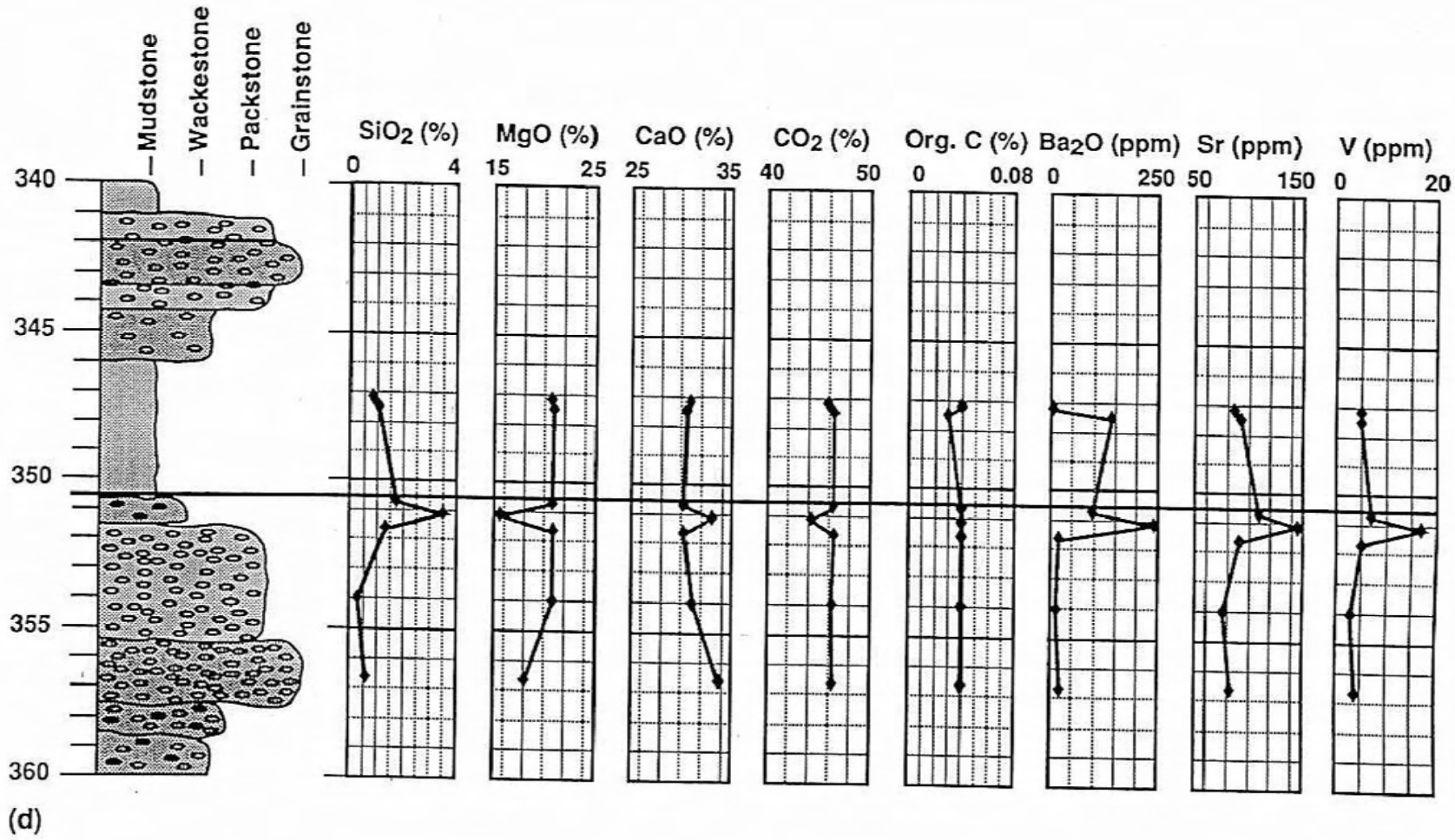

FIGURE 2d. Depth plots of key elements for each of the sampled stratigraphic intervals in the core (interval 4). Depositional textures and sedimentary structures are like those shown on Figure 1. The boundary between depositional cycles is indicated by a bold line.

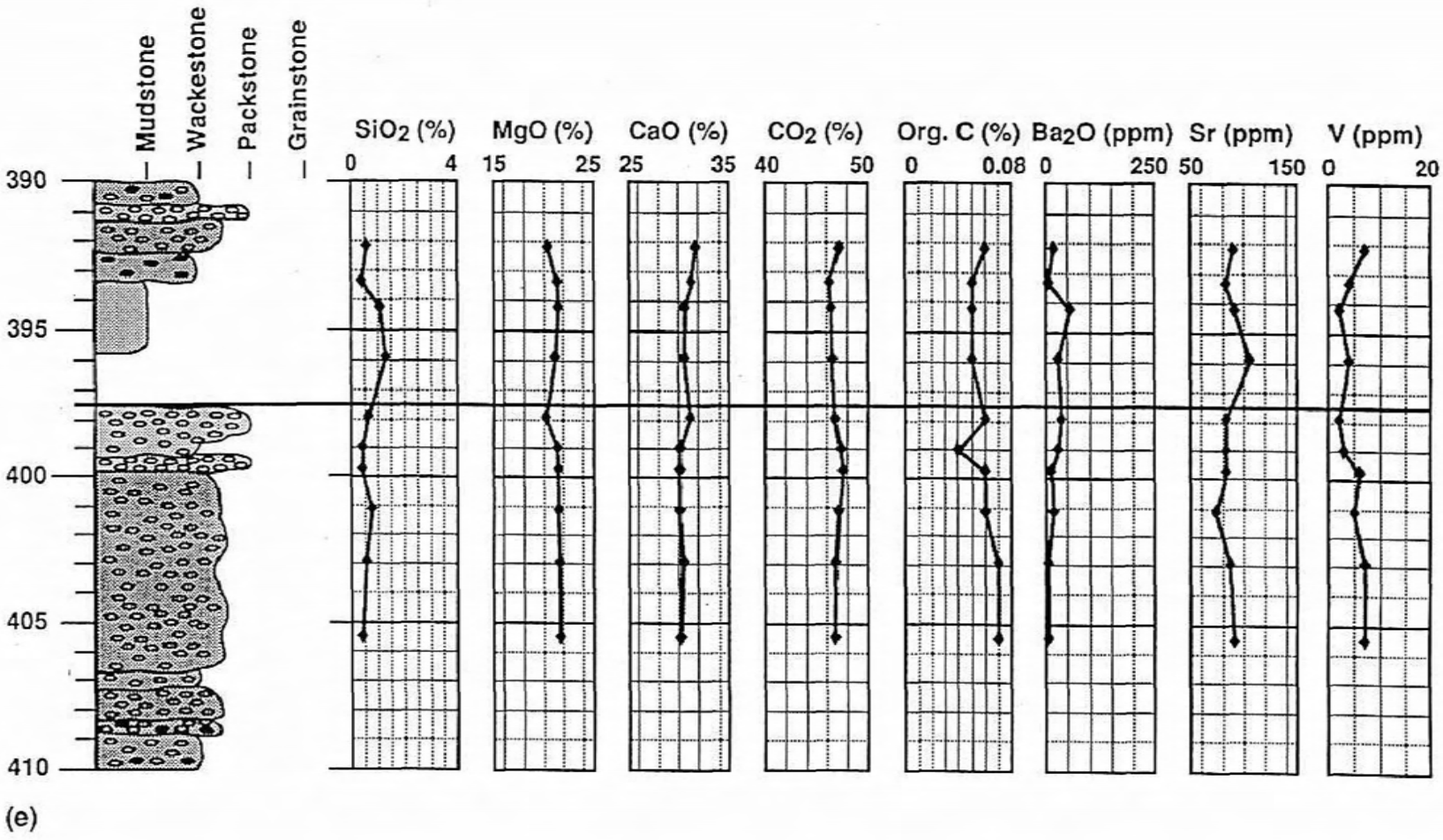

FIGURE 2e. Depth plots of key elements for each of the sampled stratigraphic intervals in the core (interval 5). Depositional textures and sedimentary structures are like those shown on Figure 1. The boundary between depositional cycles is indicated by a bold line.

Table of Eigenvectors

EigenValue:	9.5584	4.4922	1.7355	1.6396	1.2636	0.7583	0.7233	0.5869	0.5504	0.3720	0.3194	0.2584	0.1958
Percent:	41.5582	19.5313	7.5457	7.1288	5.4937	3.2969	3.1447	2.5519	2.3931	1.6172	1.3888	1.1235	0.8513
CumPercent:	41.5582	61.0895	68.6352	75.7641	81.2578	84.5547	87.6994	90.2512	92.6444	94.2616	95.6504	96.7739	97.6252
Eigenvectors:													
SiO2/Ctot	0.30452	-0.00145	0.17806	-0.03919	-0.04497	0.04555	0.05300	-0.00472	-0.08841	-0.01914	0.04124	-0.06492	0.02020
Al2O3/Ctot	0.31174	-0.04991	0.05171	0.03203	-0.01355	0.04412	0.06592	-0.24543	-0.06544	-0.00490	0.02785	-0.09472	-0.01013
Fe2O3/Ctot	0.31093	0.04486	-0.01949	0.11256	-0.11606	0.03237	0.06616	-0.04448	-0.08764	-0.02112	0.06455	-0.05956	-0.11114
MgO/Ctot	-0.17600	0.06665	0.50432	0.10748	0.06326	-0.12366	0.40583	-0.05213	-0.10041	0.11868	0.15724	0.09944	0.30149
CaO/Ctot	0.14795	-0.12822	-0.51725	-0.19790	-0.15419	0.09307	-0.21622	0.16544	0.11318	0.30901	-0.03748	0.13801	0.19494
Na2O/Ctot	0.01658	0.05469	-0.10287	0.46080	0.52963	-0.44192	-0.36566	-0.01051	-0.01096	-0.00512	0.04604	0.15391	0.16503
K2O/Ctot	0.27544	-0.08302	-0.15914	0.03254	0.13551	-0.02525	-0.11795	-0.11768	-0.17306	-0.46261	0.22742	0.12989	0.00991
TiO2/Ctot	0.31044	-0.04449	0.11301	0.03720	0.00180	-0.04021	0.02347	0.11402	0.12006	-0.06856	-0.03420	0.00657	-0.12294
Cr2O3/Ctot	0.12450	-0.02141	-0.43535	0.11551	-0.02199	-0.36154	0.67232	0.24196	-0.18000	-0.01379	-0.17118	0.08648	0.08539
Corg/Ctot	0.09064	0.37354	0.07864	-0.11781	0.26678	0.24874	-0.04210	0.05961	-0.09598	0.28107	-0.32503	0.14795	0.08207
CO2/Ctot	-0.04536	-0.27658	0.05118	0.39306	-0.40639	-0.14070	-0.01229	-0.18464	0.27044	0.25667	0.17774	0.28290	-0.28411
Ba/Ctot	0.27219	-0.05645	0.12202	0.02533	-0.20825	-0.02912	-0.16053	0.14228	-0.01319	0.16432	0.34573	-0.15395	0.66204
Sr/Ctot	0.23750	-0.16831	0.16901	0.14126	0.14304	-0.20652	-0.08283	-0.04849	0.21067	0.32200	-0.48290	-0.31282	-0.08613
La/Ctot	-0.03585	-0.34273	-0.07320	0.33375	0.16772	0.42482	0.16765	0.18360	-0.02057	0.22484	0.00988	-0.08730	0.11087
Y/Ctot	0.14331	0.20921	-0.12588	-0.09744	0.40087	0.12922	0.27949	-0.02469	0.63038	0.08096	0.44735	-0.06283	-0.12500
Zr/Ctot	0.20563	-0.04491	0.33456	-0.08314	-0.04976	-0.10800	-0.07112	0.72330	0.19045	-0.19537	-0.05040	0.24062	-0.15382
Nb/Ctot	-0.06367	-0.33839	0.02739	0.29810	0.19912	0.48132	0.02376	0.13064	-0.07020	-0.25730	-0.07237	0.04092	0.00984
Cu/Ctot	0.01523	0.32287	-0.04813	0.29805	-0.28408	0.15570	0.03764	-0.15261	0.45636	-0.37512	-0.37134	0.15087	0.36489
Pb/Ctot	0.00961	0.40579	-0.06274	0.30578	-0.13600	0.12872	-0.03118	0.18082	-0.10967	0.17255	0.13589	-0.10265	-0.08759
Zn/Ctot	-0.00685	0.38771	-0.07069	0.32541	-0.14989	0.07236	-0.12005	0.21428	-0.21917	0.04854	0.14592	-0.16514	-0.26618
Ni/Ctot	0.29987	0.08879	0.02743	0.10431	-0.00072	0.04999	0.11441	-0.18623	-0.10150	-0.03688	-0.08117	-0.18351	-0.07720
As/Ctot	0.31113	-0.07802	0.01914	-0.01871	-0.04339	0.04100	0.00172	-0.10716	-0.04130	-0.07641	-0.02616	-0.16859	-0.04458
V/Ctot	0.27662	0.06157	0.08148	-0.02899	0.05032	0.16377	0.02348	-0.19828	-0.18493	0.23148	-0.00588	0.69926	-0.06358

TABLE 3. Results of principal components analysis for the multielement geochemical data. Five principal components with eigenvalues greater than one explain 81 percent of the variance in the data.

TABLE 4. Rotated principal components show factor loadings of the chemical variables. Three components are related to depositional and diagenetic processes: Factor 1 loads on Si, Al, Fe, Ti, Ba, Ni, As, and V which we interpret to represent an introduction of detrital-clay; Factor 3 loads on Ca and Mg which we relate to dolomitization; and Factor 4 can be related to organo-metallic complexing and loads on Cu, Pb, Zn and organic carbon.

Rotated Factors

Rotated Factor Pattern	Factor1	Factor2	Factor3	Factor4	Factor5
SiO2/Ctot	0.9542196	-0.146727	-0.089344	-0.001395	-0.080165
Al2O3/Ctot	0.9364698	-0.062894	-0.252236	0.0270891	0.0366047
Fe2O3/Ctot	0.9008892	-0.075864	-0.316417	-0.231944	0.0163519
MgO/Ctot	-0.294081	0.0738517	0.8271874	-0.067693	0.0263749
CaO/Ctot	0.2150987	0.0121360	-0.855619	0.1871504	-0.167758
Na2O/Ctot	0.0121547	-0.07801	-0.002839	-0.171055	0.8375725
K2O/Ctot	0.7371453	-0.101265	-0.463877	0.1228556	0.2026882
TiO2/Ctot	0.9577617	-0.070927	-0.171856	0.0295916	0.0415398
Cr2O3/Ctot	0.1903084	0.0293414	-0.649225	-0.118698	0.1702275
Corg/Ctot	0.1888686	-0.778765	0.1363355	-0.405632	0.0591902
CO2/Ctot	0.0209988	0.9101441	0.0180181	0.0197678	0.0178051
Ba/Ctot	0.8663705	0.0813931	-0.156718	-0.030705	-0.146414
Sr/Ctot	0.7993597	0.1246948	-0.036663	0.2374115	0.2496262
La/Ctot	-0.037811	0.6040351	-0.091192	0.4009369	0.4817442
Y/Ctot	0.2785706	-0.666184	-0.190979	-0.127034	0.2550252
Zr/Ctot	0.7404062	-0.055222	0.1802179	0.1251971	-0.150057
Nb/Ctot	-0.081753	0.5757199	0.0602627	0.4466787	0.4570986
Cu/Ctot	0.0133464	-0.062975	0.0130186	-0.846743	-0.029218
Pb/Ctot	-0.034747	-0.253242	0.0449329	-0.921197	0.0903346
Zn/Ctot	-0.078783	-0.199154	0.0464523	-0.910348	0.0981135
Ni/Ctot	0.8718134	-0.199392	-0.221257	-0.239358	0.0895903
As/Ctot	0.9221381	-0.045263	-0.309174	0.0883123	-0.020266
V/Ctot	0.8141499	-0.27123	-0.148449	-0.076659	0.0138387
Std Score Coefficients					
SiO2/Ctot	0.1359139	-0.00535	0.0868474	0.0100592	-0.066062
Al2O3/Ctot	0.1122753	0.0196566	0.0023308	0.0006840	0.0059624
Fe2O3/Ctot	0.1013805	0.0714355	-0.047171	-0.106224	-0.016659
MgO/Ctot	0.0742351	0.0249483	0.3914974	-0.006215	0.0393631
CaO/Ctot	-0.084983	-0.001801	-0.417573	0.0320376	-0.142104
Na2O/Ctot	-0.017458	-0.071686	0.0176370	-0.026648	0.5931561
K2O/Ctot	0.0423239	-0.045903	-0.12862	0.0493558	0.1279206
TiO2/Ctot	0.1264960	0.0154227	0.0479724	0.0064837	0.0120525
Cr2O3/Ctot	-0.060456	0.0430746	-0.315049	-0.079026	0.0918624
Corg/Ctot	0.0075845	-0.287681	0.0900676	0.0109621	0.0960497
CO2/Ctot	0.0617058	0.4443516	0.0069337	-0.195227	-0.065331
Ba/Ctot	0.1280053	0.1145912	0.0342057	-0.056584	-0.13366
Sr/Ctot	0.1240878	0.0364962	0.1093054	0.0633190	0.1560226
La/Ctot	0.0016989	0.1647956	-0.028569	0.0429557	0.2995777
Y/Ctot	-0.02585	-0.303582	-0.053972	0.0929383	0.2227335
Zr/Ctot	0.1440772	0.0021556	0.2008600	0.0539145	-0.107361
Nb/Ctot	0.0139312	0.1388250	0.0462860	0.0741629	0.2912280
Cu/Ctot	0.0151004	0.1622788	-0.024922	-0.33709	-0.042398
Pb/Ctot	-0.001216	0.0715474	-0.013069	-0.319275	0.0580597
Zn/Ctot	-0.00519	0.0923911	-0.018263	-0.325868	0.0601789
Ni/Ctot	0.1010729	0.0032964	0.0015175	-0.074963	0.0488328
As/Ctot	0.1030853	0.0190632	-0.029005	0.0182450	-0.035111
V/Ctot	0.0962857	-0.066258	0.0365027	0.0099314	0.0099412

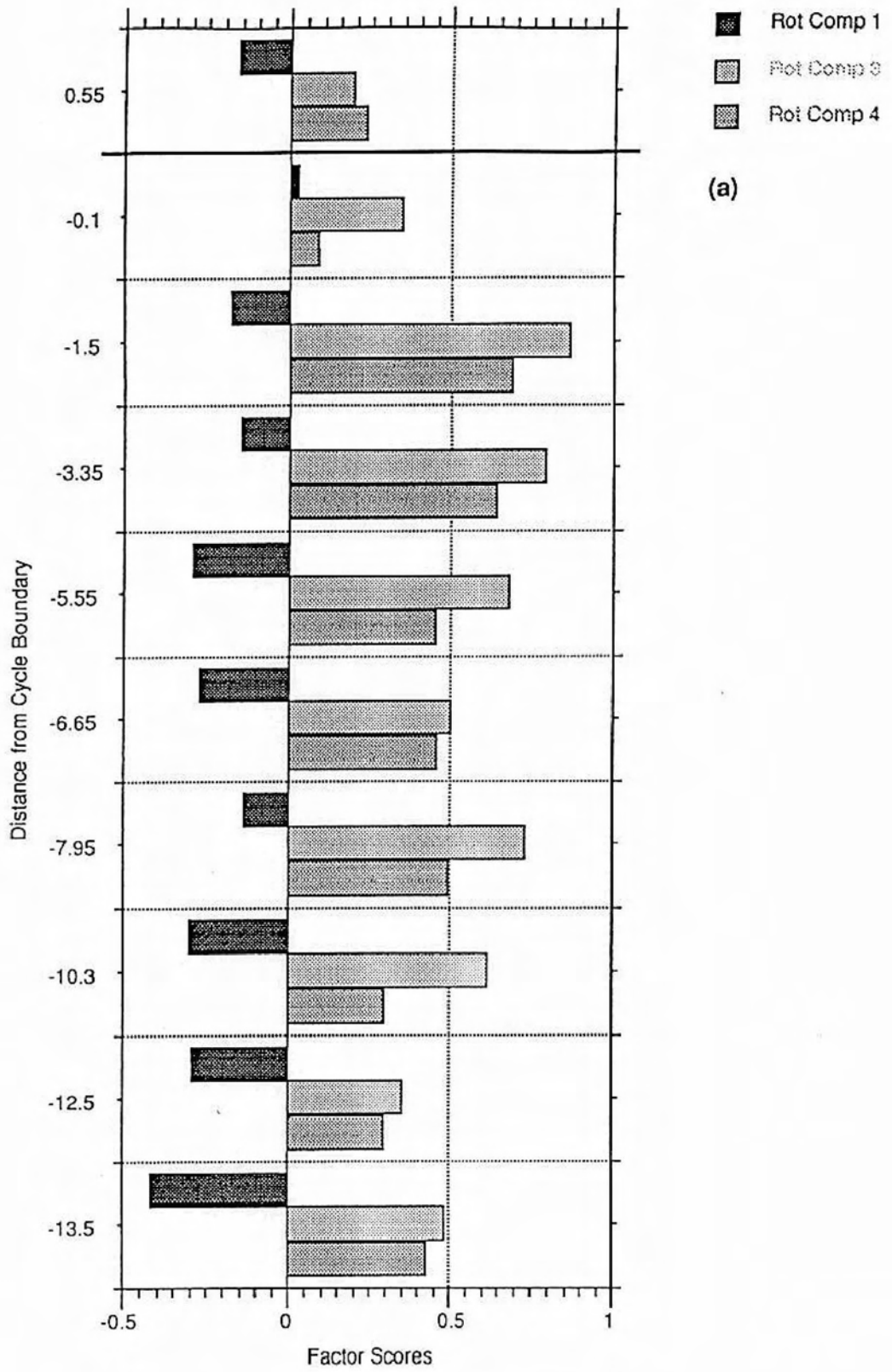

FIGURE 3a. Plots showing variations of key principal components above and below each of the five stratigraphic bounding surfaces: (a) interval 1. The bounding surface is indicated by a bold line. Rotated component 1 = detrital clay factor, 3 = dolomite factor, and 4 = organo-metallic factor.

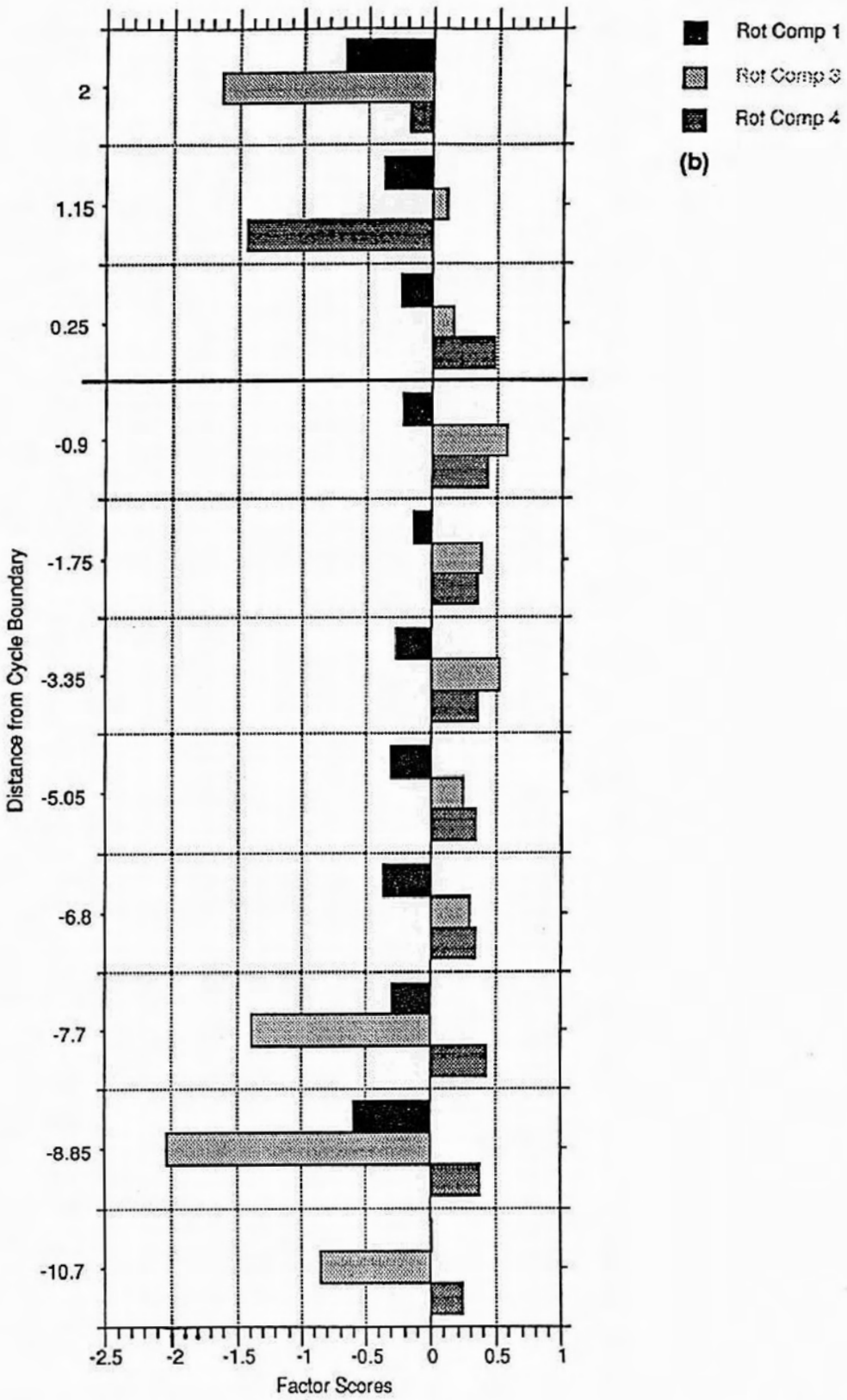

FIGURE 3b. Plots showing variations of key principal components above and below each of the five stratigraphic bounding surfaces: (b) interval 2. The bounding surface is indicated by a bold line. Rotated component 1 = detrital clay factor, 3 = dolomite factor, and 4 = organo-metallic factor.

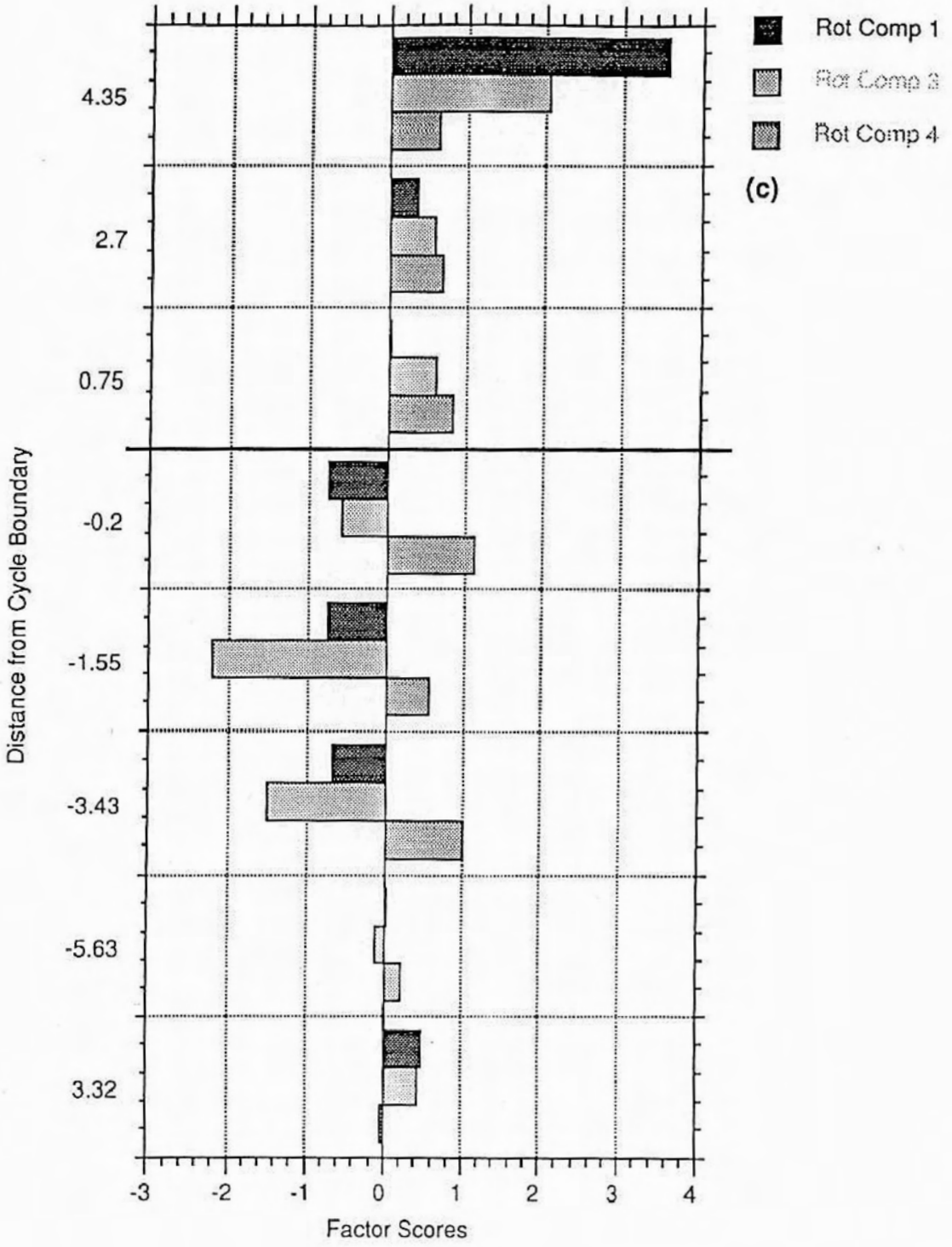

FIGURE 3c. Plots showing variations of key principal components above and below each of the five stratigraphic bounding surfaces: (c) interval 3. The bounding surface is indicated by a bold line. Rotated component 1 = detrital clay factor, 3 = dolomite factor, and 4 = organo-metallic factor.

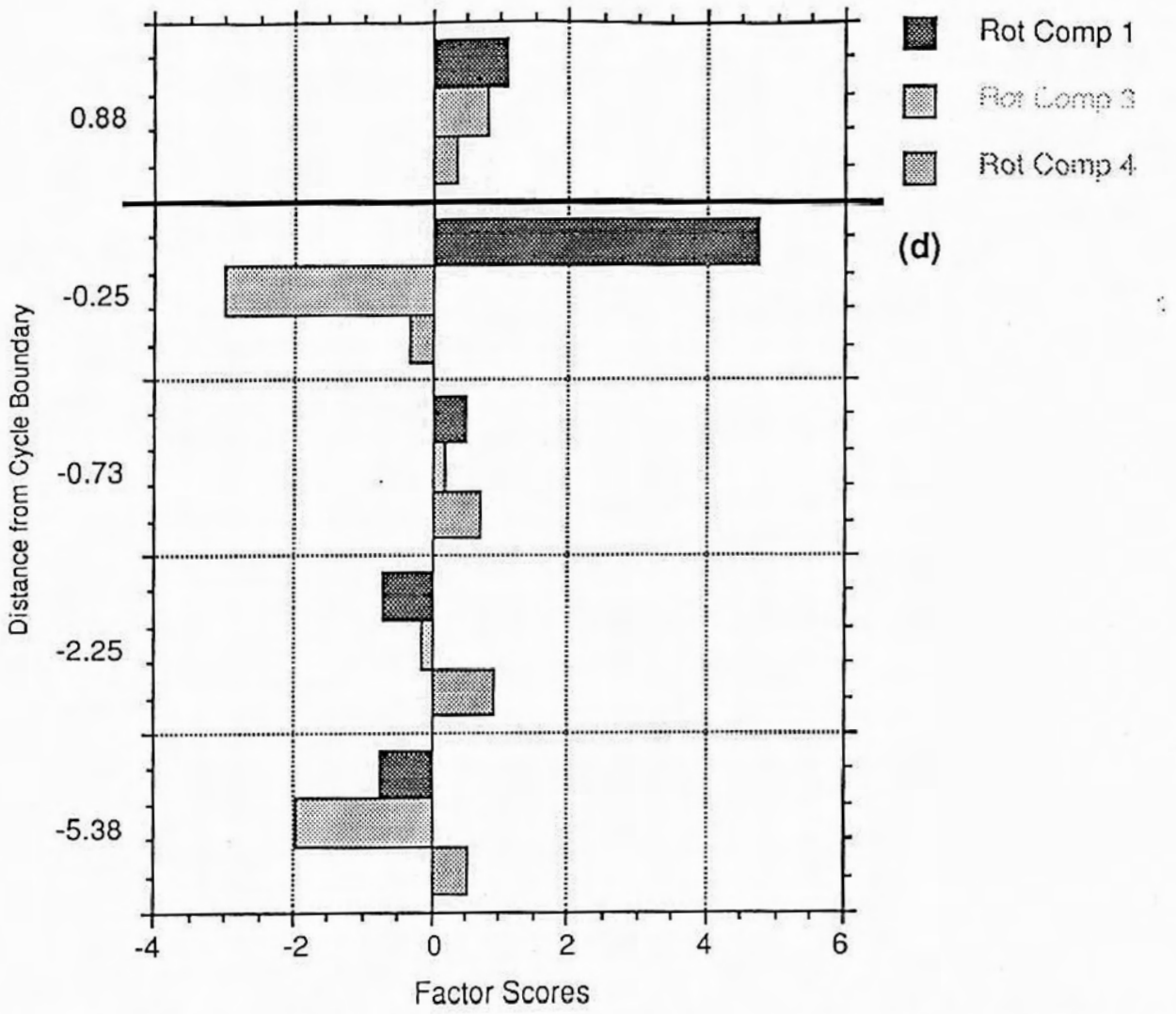

FIGURE 3d. Plots showing variations of key principal components above and below each of the five stratigraphic bounding surfaces: (d) interval 4. The bounding surface is indicated by a bold line. Rotated component 1 = detrital clay factor, 3 = dolomite factor, and 4 = organo-metallic factor.

SUMMARY

In this proof of concept study we have used multielement geochemistry and multivariate statistical analysis to supplement stratigraphic studies. Three principal components related to depositional/diagenetic processes were interpreted and used to evaluate the bounding surfaces: (1) a "detrital clay factor" which we relate to regional subaerial exposure with weathering and transportation of fine-grained clastics across the carbonate shelf; (2) a "dolomitization factor" related to various dolomite types and calcite cement content; and (3) an "organo-metallic factor" that we relate to flooding and reworking of organics from the up-dip portions of the shelf (terrigenous carbon) and improved circulation in the basin (marine carbon). Relatively high concentrations of elements associated with the "detrital clay factor" occur within two cycle boundaries and may represent a large-scale sequence boundary; a concentration of organic carbon and associated base metals coincides with a flooding surface.

The variable development of depositional cycles within hydrocarbon reservoirs, especially reservoirs contained within platform carbonates like those of the San Andres and Grayburg formations, can have a profound influence on fluid flow (Goggin and others, 1993; Grant and others, 1994; Kerans and others, 1994; Eisenberg and others, 1994). When placed into a sequence stratigraphic framework, cycle variability can be predicted. It is our hope that the chemostratigraphic methods discussed in this paper can be helpful in establishing a geologic framework and therefore predicting cycle variability. The geochemically distinct flooding surface within our interval 5 separates reservoir-scale layers with potentially different

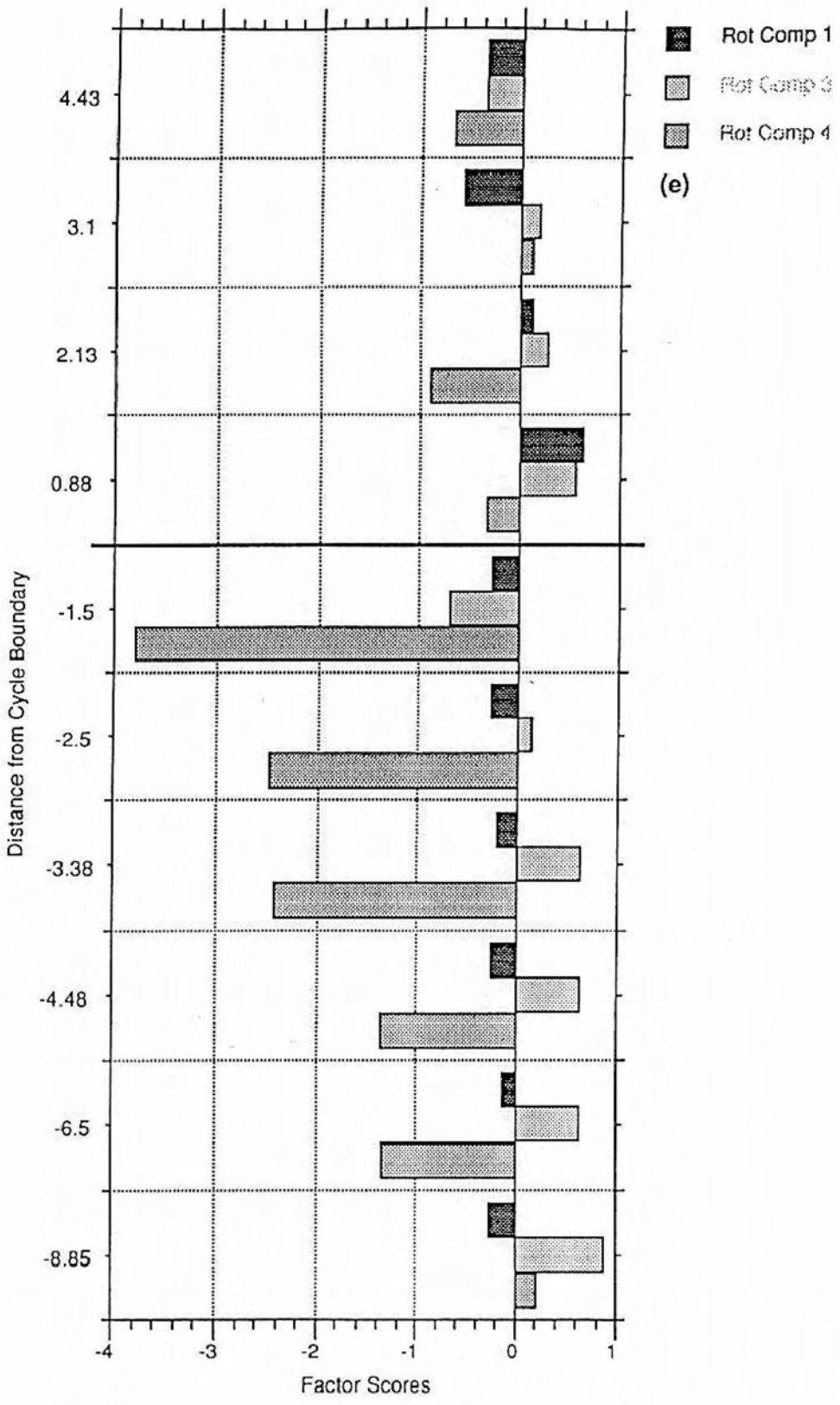

FIGURE 3e. Plots showing variations of key principal components above and below each of the five stratigraphic bounding surfaces: (e) interval 5. The bounding surface is indicated by a bold line. Rotated component 1 = detrital clay factor, 3 = dolomite factor, and 4 = organo-metallic factor.

fluid flow characteristics as shown by Eisenberg and others (1994) and is therefore a critical boundary within an outcrop analog reservoir architecture. Less distinct cycles below this surface are characterized in reservoir models discussed in by Eisenberg and others (1994) by compartmentalized flow and poor vertical sweep efficiency, whereas well-developed cycles above are characterized by a potential for early water breakthrough and relatively high vertical sweep efficiencies.

Our chemostratigraphic techniques can be used with core or cuttings samples, and once validated for the stratigraphy of a particular region, may prove to be useful in better defining a stratigraphic framework. The technique will add information to support core and outcrop studies, but more importantly it may prove to be a very valuable approach in downhole log and cuttings studies where conventional rock-based criteria for recognizing stratigraphic surfaces are difficult or impossible to use.

Comparing Figures 3a-e suggests that trends in the variation of the rotated principal components versus depth may indeed be useful in delineating sequence boundaries and flooding surfaces. Additional examples are needed to clarify if repeated systematic patterns are indeed present in our data set and to test the validity of our approach in different geologic data sets. Continuous sampling of thick intervals will be necessary to show larger scale chemostratigraphic trends and more completely characterize the relative significance of principal component variations we have observed.

REFERENCES

Eisenberg, R. A., Harris, P. M., Grant, C. W., Goggin, D. J., and Conner, F. J., 1994, Modeling reservoir heterogeneity within outer ramp carbonate facies using an outcrop analog, San Andres Formation of the Permian Basin: American Association of Petroleum Geologists Bulletin, v. 78 (9), p. 1337-1359.

Goggin, D. J., Eisenberg, R. A., Grant, C. W., and Harris, P. M., 1993, Stratigraphic controls on permeability and fluid flow patterns in ramp carbonates: an outcrop study of the San Andres Formation, New Mexico, U.S.A., *in* Eschard, R. and Doligez, B. (eds.), Subsurface Reservoir Characterization from Outcrop Observations: Proceedings of the 7th IFP Exploration and Production Research Conference, Editions Technip, Paris, p. 65-95.

Grant, C. W., Goggin, D. J., and Harris, P. M., 1994, Outcrop analog for cyclic-shelf reservoirs, San Andres Formation of Permian Basin: stratigraphic framework, permeability distribution, geostatistics, and fluid-flow modeling: American Association of Petroleum Geologists Bulletin, v. 78, p. 23-54.

Harris, P. M., Kerans, Charles, and Bebout, D. G., 1994, Ancient outcrop and modern examples of platform carbonate cycles - implications for subsurface correlation and understanding reservoir heterogeneity, *in* Loucks, R. G. and Sarg, J. F. (eds.), Carbonate sequence stratigraphy - recent developments and applications: American Association of Petroleum Geologists Memoir 57, p. 475-492.

Hovorka, S. D., Nance, H. S., and Kerans, Charles, 1994, Parasequence geometry as a control on permeability evolution: examples from the San Andres and Grayburg formations in the Guadalupe Mountains, New Mexico, *in* Loucks, R. G. and Sarg, J. F. (eds.), Carbonate sequence stratigraphy - recent developments and applications: American Association of Petroleum Geologists Memoir 57, p. 493-514.

Kerans, Charles, Lucia, F. J., and Senger R. K., 1994, Integrated characterization of carbonate ramp reservoirs using outcrop analogs: American Association of Petroleum Geologists Bulletin, v. 78, p. 181-216.

Kerans, Charles, Lucia, F. J., Senger, R. K., Fogg, G. E., Nance, H. S., Kasap, E. and Hovorka, S. D., 1991, Characterization of reservoir heterogeneity in carbonate-ramp systems, San Andres/Grayburg, Permian Basin: Reservoir Characterization Research Laboratory, The University of Texas at Austin, Bureau of Economic Geology Final Report, 245 p.

Kerans, Charles, Sonnenfeld, M. D., Fitchen, W. M., Tinker, S. W., Gardner, M. H., and Wardlaw, B. R., 1992, Styles of sequence development within uppermost Leonardian through Guadalupian strata of the Guadalupe Mountains, Texas and New Mexico, *in* Mruk, D. H. and Curran, B. C. (eds.), Permian Basin exploration and production strategies: Applications of sequence stratigraphic and reservoir characterization concepts: West Texas Geological Society Publication 92-91, p. 1-6.

Sarg, J. F. and Lehmann, P. J., 1986, Lower-Middle Guadalupian facies and stratigraphy San Andres/ Grayburg Formations, Permian Basin, Guadalupe Mountains, New Mexico, *in* Moore G. E., and Wilde, G. L. (eds.), Lower and Middle Guadalupian facies, stratigraphy, and reservoir geometries, San Andres/ Grayburg Formations, Guadalupe Mountains, New Mexico and Texas: Permian Basin Section, Society of Economic Paleontologists and Mineralogists, Publication 86-25, p. 1-35.

Sarg, J. F., Rossen, C., Lehmann, P. J., and Pray, L. C., 1988, Geologic guide to the western escarpment, Guadalupe Mountains, Texas: Permian Basin Section, Society of Economic Paleontologists and Mineralogists, Publication 88-30, 60 p.